Molecular Dynamics Simulations on Nucleic Acid Binding Polymers Designed to Arrest Thrombosis

Deniz Meneksedag-Erol[*,a,b], Jayachandran N. Kizhakkedathu[c,d,e], Tian Tang[a,f], Hasan Uludağ[a, b, g]

[a] Department of Biomedical Engineering, University of Alberta, Edmonton, AB, Canada.
[b] Department of Chemical and Materials Engineering, University of Alberta, Edmonton, AB, Canada.
[c] Centre for Blood Research, University of British Columbia, Vancouver, BC, Canada.
[d] Department of Pathology and Laboratory Medicine, University of British Columbia, Vancouver, BC, Canada.
[e] Department of Chemistry, University of British Columbia, Vancouver, BC, Canada.
[f] Department of Mechanical Engineering, University of Alberta, Edmonton, AB, Canada.
[g] Faculty of Pharmacy and Pharmaceutical Sciences, University of Alberta, Edmonton, AB, Canada.

[*] Corresponding author: Deniz Meneksedag-Erol at meneksed@ualberta.ca

Keywords: Antithrombotic polymer; Polyamine; Polyethylene glycol; Nucleic acid; DNA; Cancer-associated thrombosis; Molecular dynamics simulation.

ABSTRACT

Cancer-associated thrombosis is managed by the administration of anticoagulants and antithrombotic agents which have a high risk of inducing hemorrhagic complications. To develop safer strategies for antithrombotic therapy, *in vivo* activators of the intrinsic pathway, namely cell free nucleic acids (cfNAs: DNA and RNA) have been targeted with cationic, polyamine based polymers. The cytotoxicity of the highly cationic polymers is a major drawback for their practical use, and biocompatible alternatives are in high demand. In this study, we carried out all-atom molecular dynamics simulations to systematically examine the DNA binding of polyamine–polyethylene glycol (PEG) diblock polymers designed from biocompatible building blocks to inhibit the procoagulant activity of DNA. The differences in cationic charge, PEG chain length, and initial conformations of the polymers resulted in marked differences in their binding to DNA. We found that having an exposed cationic polyamine group is essential to polymer–DNA binding, and a certain level of electrostatic interactions is necessary to maintain the bound state. Intrachain associations between the polyamine groups and PEG chains in some cases have led to a collapsed state of the polymer that precludes binding to DNA. This self-association is mainly due to a strong hydrogen bond between polymer polyamine and PEG groups, and partly due to a partially charged semi-branched polyamine group architecture. As polymer 'masking' of DNA is thought to arrest DNA's prothrombotic activity, our findings highlight the desired structural features of the polymers for stronger DNA binding and provide insights into the design of novel antithrombotic agents.

1. INTRODUCTION

Thrombosis, the pathologic formation of an occlusive blood clot, is a serious complication of malignancy.[1,2] Cancer patients are at higher risk of developing life threatening blood clots or suffering from complications related to the use of anticoagulant drugs.[3] Multiple interrelated processes could lead to cancer associated thrombosis,[4] one of which relies on cell-free nucleic acids (cfNAs: DNA and RNA). A large body of experimental evidence suggests that cfNAs are procoagulant and prothrombotic. Owing to their anionic nature, they can contribute to thrombosis by triggering the activation of the intrinsic pathway of coagulation.[5-7] Serum cfNA levels are significantly higher in cancer patients compared to healthy individuals[8-10] and patients with benign diseases,[11] which make cfNA an attractive therapeutic target for prevention and treatment of cancer related thrombosis.

The current treatment option for cancer associated thrombosis is mainly heparin derived anticoagulants.[12] Despite their effectiveness, these drugs possess serious bleeding risks as they target the key members of the coagulation cascade. Inhibiting the *in vivo* activators of the intrinsic pathway, such as cfNAs, may potentially be a safer strategy since these molecules do not take part in the key enzymatic reactions in the coagulation cascade but rather act as potentiators of thrombosis. Cationic polymers are promising candidates in this context; they can effectively shield the negative charge of cfNAs via electrostatic interactions and arrest cfNA prothrombotic activity. A number of studies demonstrated the potential of cationic polymers as antithrombotic agents. Jain and coworkers reported that a generation 3 (G3) polyamidoamine (PAMAM) dendrimer can decrease the rate of clot formation in whole human blood, and prolong the time of vessel occlusion in *in vivo* mice models without a significant increase in blood loss.[13] Smith *et al.* identified low and high molecular weight polyethylenimine (PEI), spermine, and generation 1 (G1) PAMAM

dendrimer as potent inhibitors of prothrombotic activity of polyphosphate (polyP), which is another naturally occurring procoagulant molecule.[14-17] Among these polymers, G1 PAMAM dendrimer effectively decreased the thrombus size and inhibited fibrin accumulation *in vivo*.[16]

Despite the successes of PEI and PAMAM polymers as antithrombotic agents, their toxicity is a major drawback to their practical use. Unshielded cationic charges of these polymers promote undesired interactions with blood cells, proteins and cellular membranes, reducing their biocompatibility.[18-21] In search for safer antithrombotic polymer alternatives, non-toxic universal heparin reversal agents (UHRAs) have recently attracted attention.[22,23] UHRAs are a family of dendritic polymers originally designed as synthetic heparin antidotes by Kizhakkedathu and coworkers.[24,25] Their structure comprises of a dendritic polymer core functionalized with cationic heparin binding groups, and shielded by short polyethylene glycol (PEG) chains to increase biocompatibility. UHRA compounds carrying a different number of trivalent cationic groups (R, also known as heparin binding group) were shown to delay polyP-induced clot formation while exerting much less toxicity than protamine and PEI, and less bleeding side effects compared to heparin based anticoagulants.[22] Although UHRA compounds are not designed to inhibit either polyP or RNA specifically, their antithrombotic activity against these molecules is significant. It is expected that they maintain inhibitory potency toward DNA given the structural similarities between polyP, RNA, and DNA. However, how they interact with DNA is currently unknown.

In this study, we investigated DNA binding of polymers which are designed based on the building blocks of UHRA compounds, comprising a PEG-based chain attached to a cationic R group. We aim to elucidate the molecular level details of polymer–DNA binding and identify the structural features of polymers affecting interactions with DNA. Toward this aim, we carried out all-atom molecular dynamics (MD) of model compounds varying in PEG-based chain length as

well as size, charge, and architecture of the R group. A molecular level understanding of the polymer–DNA interactions is crucial to advance the design of polymeric structures displaying superior DNA binding. The structure–function relationships uncovered in this work will form the basis of the studies in designing UHRA compounds to arrest the prothrombotic activity of DNA.

2. METHODS

2.1. Simulated Systems

The simulated DNA is Drew-Dickerson dodecamer, a prototypical 24 nucleotide B-DNA duplex with the sequence of d(CGCGAATTCGCG)$_2$. It carries a total charge of –22 in the fully deprotonated state. The initial structure of the DNA is adopted from our previous study.[26] The polymers explored in this study are composed of a PEG-based chain, and a cationic polyamine block (R). Two different lengths for the PEG chain were studied where the number of repeating PEG monomer units (n) are 11 and 22 (Figure 1a). In addition, we investigated four different polyamine groups, linear R1, semi-branched R2a and R2b, and branched R3, comprising 3, 4, 4 and 7 tertiary amine groups, respectively (Figure 1b). R2a and R2b share the same tertiary amine composition and architecture, and differ only by a –CH_2-CH_2– group that precedes the first tertiary amine, which is present in R2b and absent in R2a. R2a also corresponds to the R group of the UHRA compounds previously studied by Travers and coworkers.[22] The charges of the polyamine groups under physiological conditions are +3, +3, +3 and +7, respectively, for R1, R2a, R2b and R3, making the R1 and R3 fully protonated, and R2 (R2a and R2b) partially protonated. For the discussion herein, the polymers are named with the PEG-based chain identifier, “s” for short (n=11) and “l” for long (n=22), appended to “PEG”, followed by the name of the polyamine group, R. For example, polymer PEGs-R1 is composed of a short PEG-based chain and the polyamine group R1. CHARMM36 all-atom force field[27] was used for DNA. The parameterization of the

polymers was carried out by following CHARMM general force field (CGENFF) methodology,[28] and the details are given in the Section S1 in Supporting Information.

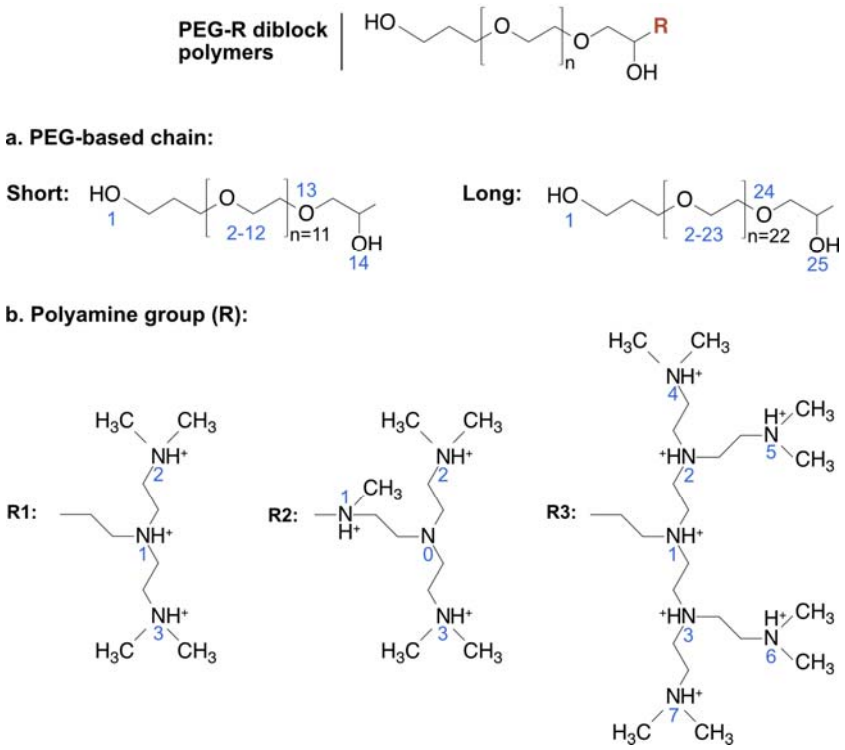

Figure 1. Chemical structures of the simulated polymers. **(a)** The length of the PEG chain is varied by changing the number of repeating PEG monomer units (n). The short PEG chain (n = 11) will be referred to as PEGs, and the long PEG chain (n = 22) will be referred to as PEGl. The numbering of the O atoms is indicated with numbers in blue (1-14 for short and 1-25 for long chain) shown next to each O atom. **(b)** The polyamine groups consist of a different number (3, 4 and 7 for R1, R2 (R2a and R2b) and R3, respectively) of tertiary amines. The numbering of the N atoms is indicated with numbers in blue shown next to each N atom. Number 0 stands for the unprotonated N atom, while numbers 1-7 indicate the protonated Ns. The protonation sites at physiological pH are marked with "+".

For the equilibration of each polymer, first its initial structure was placed in a CHARMM-modified TIP3P water[29] box, and neutralized with the addition of a proper amount of Cl^- ions. The polymer was then subjected to two independent MD runs, each consisting of a 10 ns (restrained) and a 100 ns (free) simulation. The polymers were initially built in the fully extended conformation (Figure S1 in Supporting Information). During the equilibration simulations, the PEG-based chain

was observed to be highly dynamic. Taking the radius of gyration (R_g) of the PEG chain as a metric to assess its solvation in water, it was seen that the PEG chain repeatedly fluctuated between extended (higher R_g) and collapsed (lower R_g) states (Figure S2 in Supporting Information). In addition, from the visual examination of the simulations, each polymer was observed to visit and exchange between two distinct conformations: one in which the polyamine group is exposed to solvent without part of the PEG chain in close proximity (referred to as the "extended conformation"), and the other in which the PEG chain wraps around the polyamine group to some extent, shielding its cationic charge (referred to as the "shielded conformation"). To quantify the lifetime of these two conformations during the polymer equilibration simulations, we defined the conformation as "shielded" if there is at least one polyamine N atom within 4 Å (cut off distance for a close contact to be formed) of any PEG O. The time series of the number of polyamine N atoms in close contact with PEG Os are given in Figure S3 in the Supporting Information. PEG-R2a polymers displayed a permanent contact, that is there is one N atom in close contact with PEG chain at all time. The reason for the existence of such a permanent contact will be addressed later. If we were to follow the same definition, the PEG-R2a polymers would be "shielded" in the entirety of the simulations. Therefore, only in R2a systems, we defined the shielded conformation in which there are at least 2 N atoms in close contact with any PEG O atom. Table S1 lists the life times of the extended and shielded conformations in the 100 ns long polymer equilibration simulations.

To capture the potential influence of these two polymer conformations on binding to DNA, polymer equilibration simulation trajectories were visually examined to choose one extended and one shielded conformation for each polymer. The naming of the polymers was updated to include the polymer conformation identifier; "e" for extended and "s" for shielded, appended to the

previously assigned names of the polymers. The conformations of the polymers shown in Figure 2 were used as initial structures in their subsequent DNA binding study. In each simulation, the polymer was placed at a center of mass (COM) distance of 17 Å from the DNA on the major groove side, and oriented so that its polyamine group faced DNA. The initial configurations of the polymer–DNA simulation systems are shown in Figure S4 (Supporting Information). To distinguish the polymer–DNA systems from the single polymer systems, the word "DNA" was added to the name of the polymers. For example, system PEGs-R1_e–DNA is composed of a polymer with a short PEG chain and polyamine group R1 in extended conformation, and a DNA molecule. Each polymer–DNA system was solvated in a CHARMM-modified TIP3P water box[29] with a 15 Å distance from all edges of the simulation box, and ionized with the addition of 150 mM NaCl to mimic the physiological conditions (**Error! Reference source not found.**). It was then simulated for 10 ns (restrained) + 150 ns (free).

Table 1. Details of the PEG-R–DNA simulation systems.

System	Number of water molecules	Number of NA^+/Cl^-	Simulation box size ($Å^3$)
PEGs-R1_e–DNA	6949	39/20	63x51x74
PEGs-R1_s–DNA	6900	39/20	63x51x74
PEGs-R2a_e–DNA	6868	38/19	62x51x74
PEGs-R2a_s–DNA	6980	39/20	63x51x74
PEGs-R2b_e–DNA	6822	38/19	62x51x74
PEGs-R2b_s–DNA	7056	39/20	64x51x74
PEGs-R3_e–DNA	7772	37/22	70x51x74
PEGs-R3_s–DNA	7228	35/20	66x51x74
PEGl-R1_e–DNA	7323	40/21	64x51x76
PEGl-R1_s–DNA	7255	40/21	66x51x74
PEGl-R2a_e–DNA	6986	39/20	64x51x74
PEGl-R2a_s–DNA	6923	39/20	63x51x74
PEGl-R2b_e–DNA	7342	40/21	67x51x74
PEGl-R2b_s–DNA	6923	39/20	63x51x74
PEGl-R3_e–DNA	8017	38/23	65x57x74
PEGl-R3_s–DNA	7554	36/21	66x51x76

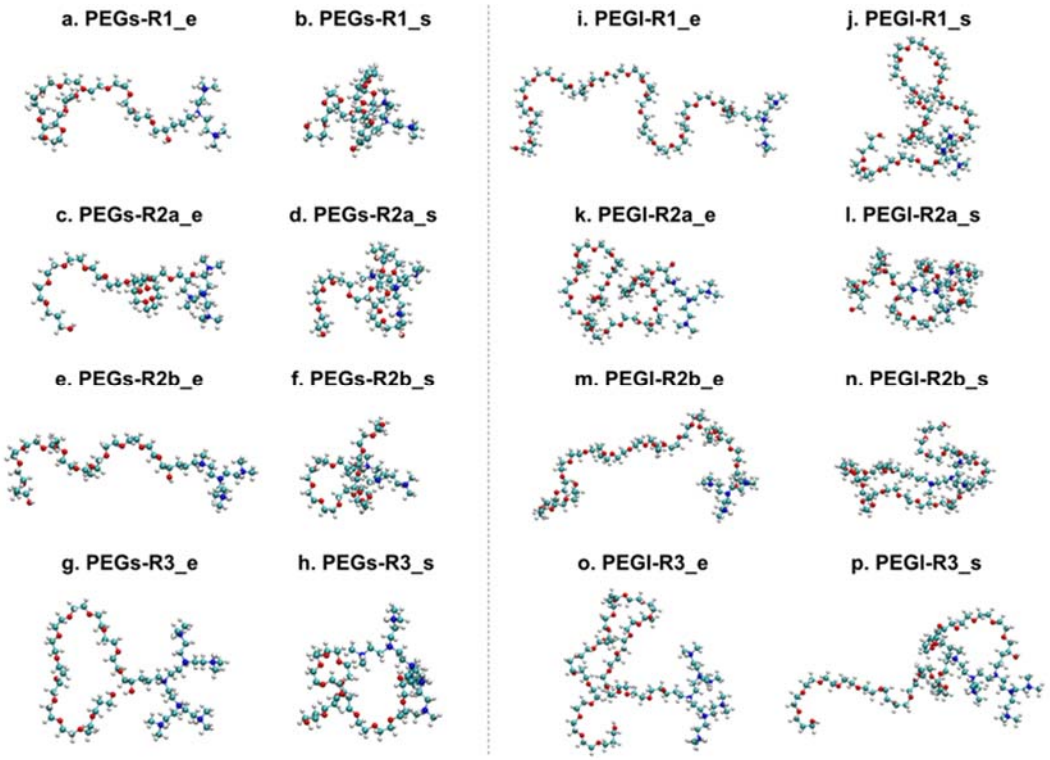

Figure 2. The extended (left) and shielded (right) conformations of **(a, b)** PEGs-R1, **(c, d)** PEGs-R2a, **(e, f)** PEGs-R2b, **(g, h)** PEGs-R3, **(i, j)** PEGl-R1, **(k, l)** PEGl-R2a, **(m, n)** PEGl-R2b, **(o, p)** PEGl-R3. For clarity, water and ions are not shown. The color coding of the atoms is as follows: cyan, C; red, O; blue, N; white, H. Each conformation is selected from an independent 100 ns equilibration simulation of the polymer in explicit water.

2.2. Simulation Details

All simulations were performed with MD package of NAMD[30], with a time step of 2 fs, periodic boundary conditions (PBC), particle mesh Ewald (PME)[31] for full electrostatics, a cut-off of 12 Å for van der Waals and pairwise interactions, and SHAKE algorithm[32] to constrain the bonds involving H atoms. First, each system was minimized for 5000 steps, followed by gradual heating from 0 K to 300 K within 20 ps, with a harmonic restraint of 10 kcal/mol·Å^2 on the non-H atoms of the solute(s). Keeping the restraint on these non-H atoms, the system was further simulated for 10 ns. The restraint was then removed, and NPT simulation was performed for 100 ns (single polymer systems) or 150 ns (polymer–DNA systems). Langevin dynamics thermostat

with thermostat damping coefficient of 10 ps^{-1} for all non-H atoms was used for temperature control. Pressure control was achieved with Nosé−Hoover−Langevin barostat with damping time scale of 100 fs and Langevin piston oscillation period of 200 fs. Simulation trajectories were visualized and analyzed with VMD.[33] Unless otherwise stated, the average values were obtained from the final 50 ns of the simulations.

3. RESULTS AND DISCUSSION

Visual examination of DNA binding simulations of the polymers comprising R1, R2a and R3 polyamine groups (Figure 3) shows that polymers bind DNA mainly through the interactions with the major groove and end regions of the DNA helix, with some transient interactions observed in the minor groove. An interesting observation is the poor DNA binding exhibited by three out of four systems comprising the R2a polyamine group (Figure 3d, i, j) as evidenced by the separation from the DNA. Such a separation was not observed in any of the systems with R1 and R3, suggesting polymer architecture plays a role in DNA binding. To understand the differences between the DNA binding performance of the polymers, we quantify polymer−DNA binding, and explore the mechanisms and structural features of the polymers affecting their binding behavior.

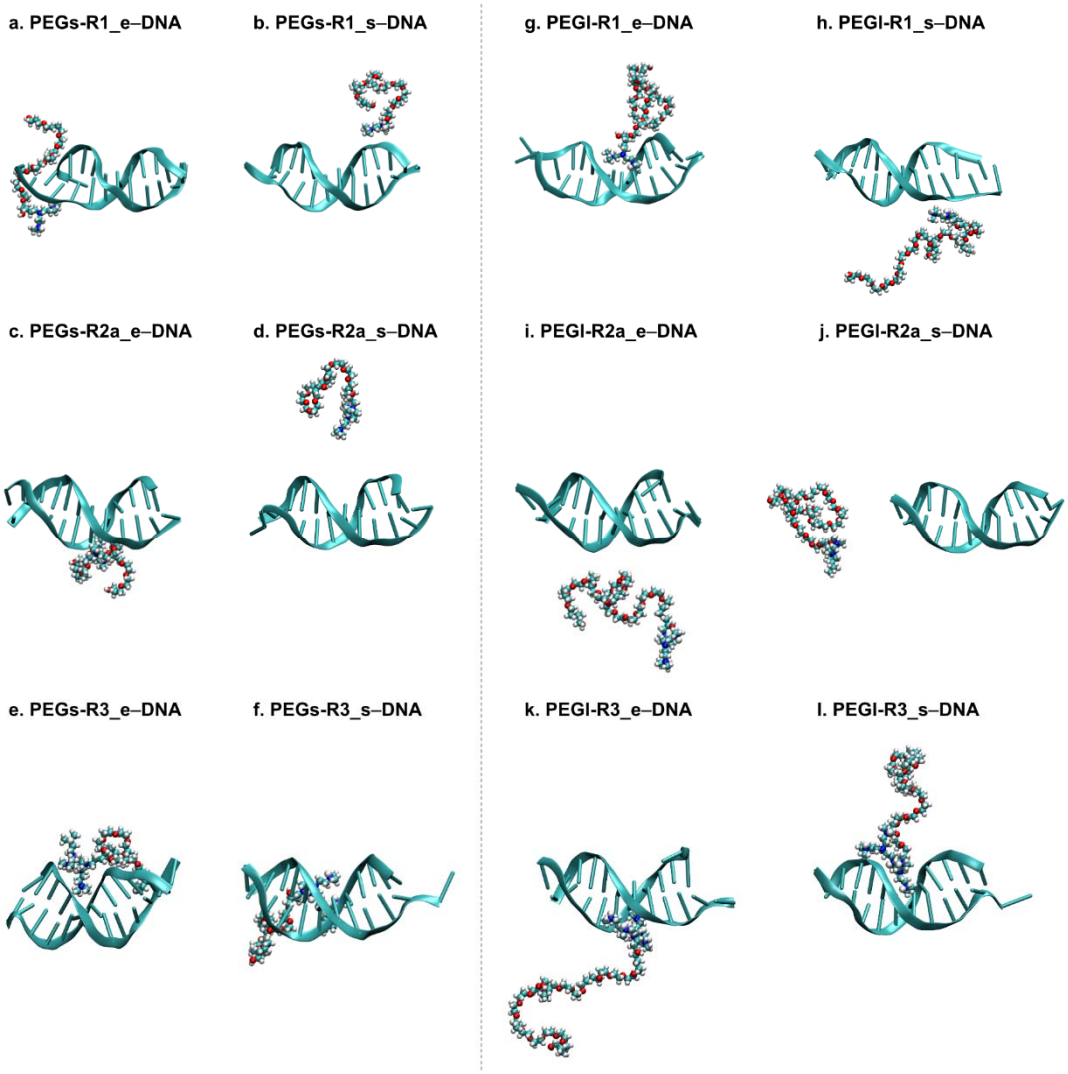

Figure 3. Final configurations from 150 ns DNA binding simulations of the polymers comprising R1 **(a, b, g, h)**, R2a **(c, d, i, j)**, and R3 **(e, f, k, l)** polyamine groups. DNA duplex is shown in cyan. The color coding of the polymer atoms is as follows: cyan, C; red, O; blue, N; white, H. Water and ions are not shown for clarity.

3.1. Polymer–DNA Binding

We first monitored and compared the interactions of the polymer polyamine and PEG groups (as defined in Figure 1) with DNA. To do so, we defined a cut-off distance of 4 Å for a close contact to be formed between DNA electronegative atoms N/O and polymer polyamine N or PEG O atoms. We previously reported 4 Å as the distance within which a direct H-bond can be formed

between DNA N/O and the amine groups of PEI;[26] as the polymer polyamine groups investigated in this study have structural similarity to PEI, we adopted 4 Å as the cut-off distance. For consistency, we followed the same definition to quantify the polymer PEG chain–DNA interactions. The contribution of the PEG chain to polymer–DNA binding was generally weak (Figures S5 and S6 in Supporting Information). These findings are consistent with a recent simulation study by Mafi and coworkers where the Os in the repeating PEG monomer units did not exhibit interactions with polyP, hence their contribution to polyP binding was insignificant.[34] Therefore, we will focus on the interactions made by the polyamine group when assessing the binding of polymers to DNA.

In Figure 4, we plot the average number of polyamine Ns in close contact with DNA N/O vs. the total number of Ns in the polyamine group. For R1 and R3, the number of Ns closely interacting with the DNA increases almost proportionally with the increase in the number of Ns in the polyamine group from 3 to 7, irrespective of the polymer initial conformation (extended vs. shielded) or PEG chain length (short vs. long). The strength of the interactions between the R2a and DNA, on the other hand, was observed to be contingent both on the length of the PEG chain and polymer initial conformation. Among the R2a polymers having initial conformations in the extended state, the one with shorter PEG chain shows slightly increased interactions with DNA when compared to the corresponding system with R1. Inversely, extending the PEG chain length resulted in little to no contacts with DNA (Figure 4). Neither of the R2a systems having initial conformations in the shielded state displayed better polymer–DNA binding when compared to the corresponding systems of R1. This indicates a strong structural restraint impacting the DNA binding strength of the R2a systems; the polymers comprising R2a should simultaneously possess a short PEG chain and an initial extended conformation to be able to bind DNA as strongly as R1.

All other combinations involving longer PEG chain and/or shielded initial conformation diminished DNA–R2a interactions. In fact, some of these combinations, PEGs-R2a_s, PEGl-R2a_e, and PEGl-R2a_s, led to separation from DNA (Figure 3d, i, j) (at 108, 45, and 132 ns, respectively (Figure S5b, e; Supporting Information). Given the equal cationic charge of the R1 and R2a, it is interesting to see that DNA binding of R2a is not as stable and strong as that of R1 in most of the cases. The mechanism behind this observation will be explored in Section 3.2.

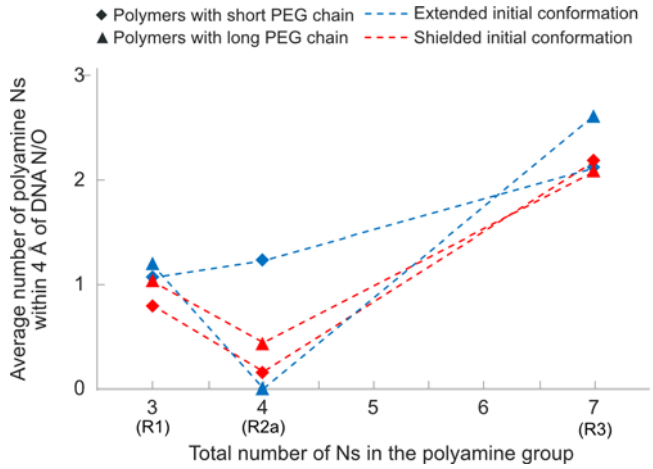

Figure 4. Number of Ns within 4 Å of DNA N/O as a function of the total number of Ns in the polyamine group, averaged over the final 50 ns of the simulations. The polymers with short and long PEG chains are represented with diamond and triangle symbols, respectively. The extended and shielded polymer initial conformations are given in blue and red, respectively.

Figure 4 demonstrates that increase in the cationic charge of the polyamine group facilitates better DNA binding, indicative of the electrostatic nature of the polymer–DNA interactions. Further analysis of our simulation systems (Figure S7, Supporting Information) has shown that binding of polyamine group to DNA is driven by the interactions with DNA backbone phosphate Os, O1P and O2P, consistent with previous reports on DNA binding to oligoamines[35-39] and PEI[26,40,41]. Weaker interactions with the phosphate esteric Os, O3′ and O5′, and base N/O was

observed in almost all systems. The DNA sugar ring O, O4′, showed little to no interactions with the polyamine groups of the polymers.

R1, R2a, and R3 differ in their architecture and nitrogen content. In order to characterize the DNA binding pattern of the individual amines, we examined the percentage of time over the final 50 ns of the simulations in which each N atom of the polyamine group interacts with DNA as defined by the 4 Å close-contact threshold (**Figure *5***). In the systems with R1 (**Figure *5***a), N1 forms the highest amount of DNA contact, followed by N2, and N3. In the systems with R2a (**Figure *5***b), the ability of N1 to interact with DNA is significantly impeded, and the interactions were mostly shifted towards N2 and N3. N0, the unprotonated N, displayed little to no interactions with DNA. It is possible that R1 aligns itself with the DNA backbone to form a strong contact through N1, while also augmenting the interactions by N2 and N3. In the R2a systems, however, the presence of an unprotonated N between the charged amines might regulate the positioning of the polyamine group to maximize the number of protonated Ns in close contact with DNA, such that the polyamine group preferably positions itself to interact with DNA through N2 and N3, instead of N1. Despite this preferential orientation, the level of DNA contact made by N2 and N3 is still poor in some of the systems, particularly in PEGs-R2a_s and PEGl-R2a_s, suggesting that there are other possible unfavorable structural features of R2a with regards to polymer–DNA binding. We will explore such features in detail in Section 3.2.

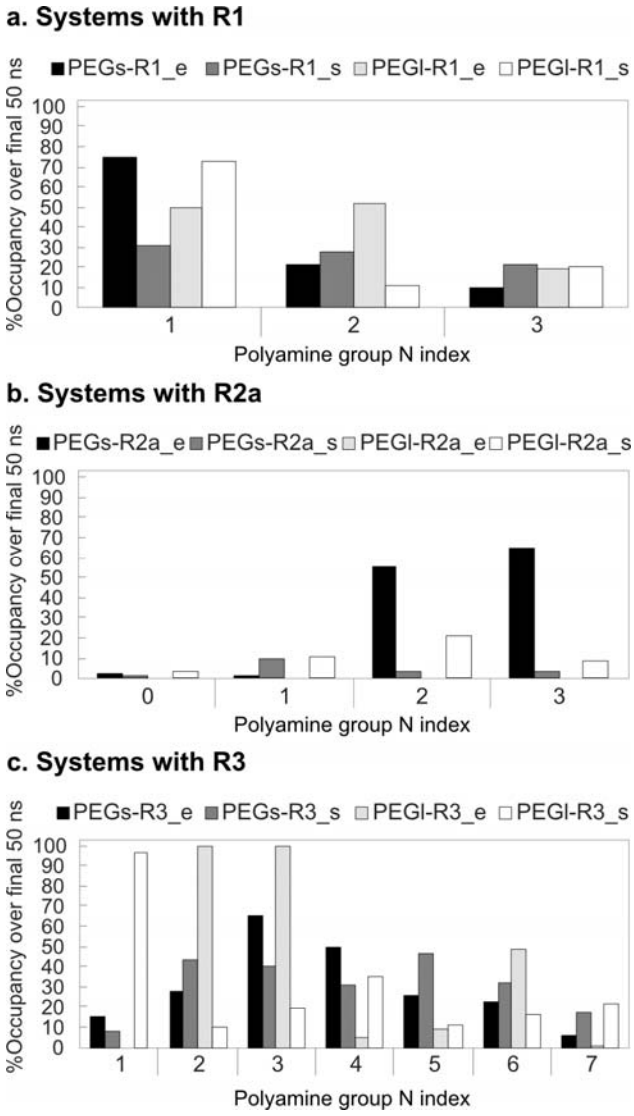

Figure 5. Percentage of time in which nitrogen atoms of the polyamine groups are in close contact with DNA N/O in the final 50 ns of the simulations with **(a)** R1, **(b)** R2a, and **(c)** R3. 100% corresponds to a state where a given N atom is in close contact with at least one DNA N/O atom at all times over the final 50 ns, where 0% represents the case of no interactions (i.e., no contact within 4 Å). The numbering of the nitrogen atoms of the polyamine groups is given in Figure 1b.

When assessing binding of R3 to DNA (Figure 5c), we investigated R3 in three regions: N2, N4, and N5 form one end of the group; N3, N6, and N7 form the other end; and N1 is the connection point. The polymers with short PEG chain interact with DNA mainly through the two ends, and N1 acts as the hinge point regulating the orientation of the two end groups. The initial

conformation of these polymers did not affect their overall DNA binding pattern, however, there exist some differences in the amount of interactions displayed by individual amines between the extended and shielded initial conformations. Polymers comprising a longer PEG chain showed a different R3–DNA binding pattern where one or two nitrogens interacted with DNA predominantly as opposed to the more dispersed distribution observed in the polymers with shorter PEG chains. For example, N2 and N3 in PEGl-R3_e, and N1 in PEGl_R3_s dominate other amines by being in close contact with DNA at all times over the final 50 ns. Moreover, in the presence of long PEG chain, R3–DNA binding became susceptible to the changes in the initial conformation of the polymers. While PEGl-R3_e exhibited the same DNA binding profile where interactions are made through the two end groups with N1 as the connection point, N1 no longer acts as the hinge in PEGl-R3_s, and significantly takes part in DNA binding. Following N1 are again the two end groups. Although the PEG chain itself does not interact with DNA, our results suggest that it may affect polyamine–DNA binding profiles. The motions of the polyamine and PEG blocks are coupled to some extent as they are covalently bonded and neither are allowed to move freely. PEG chain is well-solvated due to its high hydrophilicity, and extending its length will bring an increased range of motion, thereby increasing the mobility of the polyamine group. This may result in a decreased number of contacts with DNA. Such a decrease is also expected if a fraction of the amine groups is initially shielded by the long PEG chain, posing a barrier to the strong interactions with DNA.

From our detailed analysis of the polymer–DNA interactions, it is evident that the strength and pattern of polymer binding to DNA differ significantly with changes in the architecture of the polyamine group, length of the PEG chain, and initial polymer conformation. However, the mechanisms underlying these drastic changes in the DNA binding performance of the polymers

were not immediately clear from the current observations. We next direct our efforts to uncover the structural and mechanistic details regulating the polymer–DNA binding.

3.2. Mechanisms Governing the DNA Binding Performance of the Polymers

3.2.1. The effect of polymer intrachain associations

The fact that only the polymers comprising R2a were separating from DNA points to a structural and/or conformational restraint preventing the R2a systems from forming and/or maintaining adequate interactions with DNA. This led us to analyze the conformations of the polymers throughout their DNA binding simulations. First, we focused on the self-association within the polymers by monitoring the interactions formed between the polyamine Ns and PEG Os. We again adopted the 4 Å as the cut-off distance for defining a close contact. Irrespective of the polymer initial conformation or the length of the PEG chain, systems with R1 and R3 demonstrated weak transient intrachain associations, which were deemed negligible (Figure S8a, d, c, f; Supporting Information). Systems with R2a, however, displayed elevated levels of intrachain contacts (except for PEGl-R2a_e where the intrachain interactions are observed in a transient fashion), and intrachain associations were even more pronounced in the shielded initial conformations (Figure S8b, e; Supporting Information).

Monitoring the intrachain associations revealed an unexpected permanent contact between the polyamine and PEG blocks in the PEG-R2a polymers, where one N atom of the polyamine group was in close contact with the PEG chain at all times (Figure S7b, Supporting Information). Such a behavior was not seen in any other polymer–DNA systems. The maintenance of this permanent contact irrespective of the polymer initial conformation or PEG chain length suggests that this intrachain interaction is an inherent characteristic of the R2a polymers. To identify which particular N atom was responsible for this permanent interaction, we examined the contacts made

by individual Ns by tracking the percentage of time in which they are in close contact with any PEG O within the final 50 ns of the simulations (Figure 6). In the systems with R1 and R3, polyamine Ns interacted with the PEG Os at most 7% of the time, corroborating the lack of intrachain associations in these systems. In the systems with R2a, we found that the individual N atom making the permanent contact with the PEG chain was N1, which is the N atom immediately adjacent to the PEG chain. Following N1 are N0, N3, and N2, ordered from the most to least interacting.

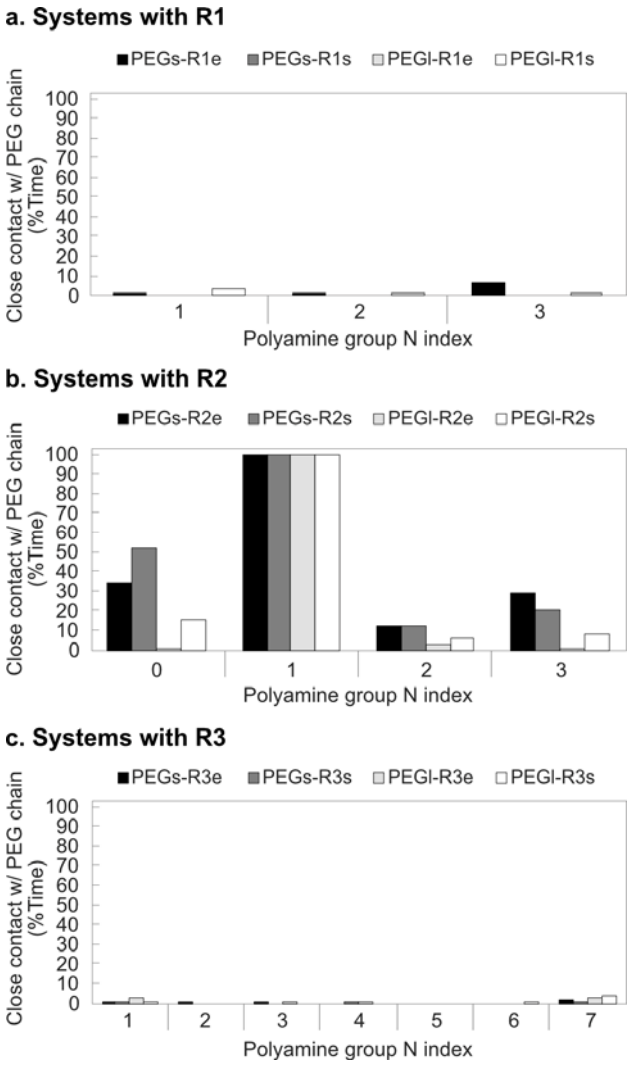

Figure 6. Percentage of time in which polyamine Ns are in close contact with PEG Os in the final 50 ns of the simulations with the polymers comprising **(a)** R1, **(b)** R2a, and **(c)** R3. The numbering of the nitrogen atoms of the polyamine group is given in Figure 1b.

We next explored the radial distribution function (RDF) of the PEG Os around polyamine Ns (Figure 7). Firstly, the initial conformation of the polymers did not significantly affect the distribution of PEG Os around polyamine Ns; i.e., given a type of polymer, the RDF peak positions are very similar between the extended and shielded initial polymer conformations. There exist some differences in the height of the RDF peaks for different polymer initial conformations: particularly, in the systems with PEGs-R1 and PEGs-R2a, extended initial conformations

demonstrated higher RDF peaks than the shielded, suggesting that polymer initial conformation can influence the probability of finding a PEG O within short distances from a polyamine N. Secondly, increasing the length of the PEG chain decreases the probability of finding a PEG chain O within short distances from the polyamine group, as evident from the reduced RDF peak height in the polymers with long vs. short PEG chains. This effect is most significant for the polymers comprising R2a.

To identify the interactive regions of the PEG chain responsible for the intrachain associations, the locations of the first two RDF peaks were examined. For all systems, the RDF peak locations are mostly preserved when the length of the PEG chain is increased; therefore, for the discussion herein, the comparison will be made among the polymers with short PEG chains. In both R1 and R3 systems, the first peaks are located at ~4.5 Å and 5.25 Å, respectively. In the systems with R2a, the location of the first peaks shifted to shorter distances, ~3 Å and 4.25 Å, respectively, indicating that PEG Os can be found within a shorter range of the polyamine Ns. Moreover, the intensity of the peaks is significantly increased in the R2a systems, particularly when the PEG chain is short (note the change in the y-scale in PEGs-R2a, Figure 7b), suggesting an increased probability of finding PEG Os within proximity of the polyamine Ns, which translates into higher intrachain associations.

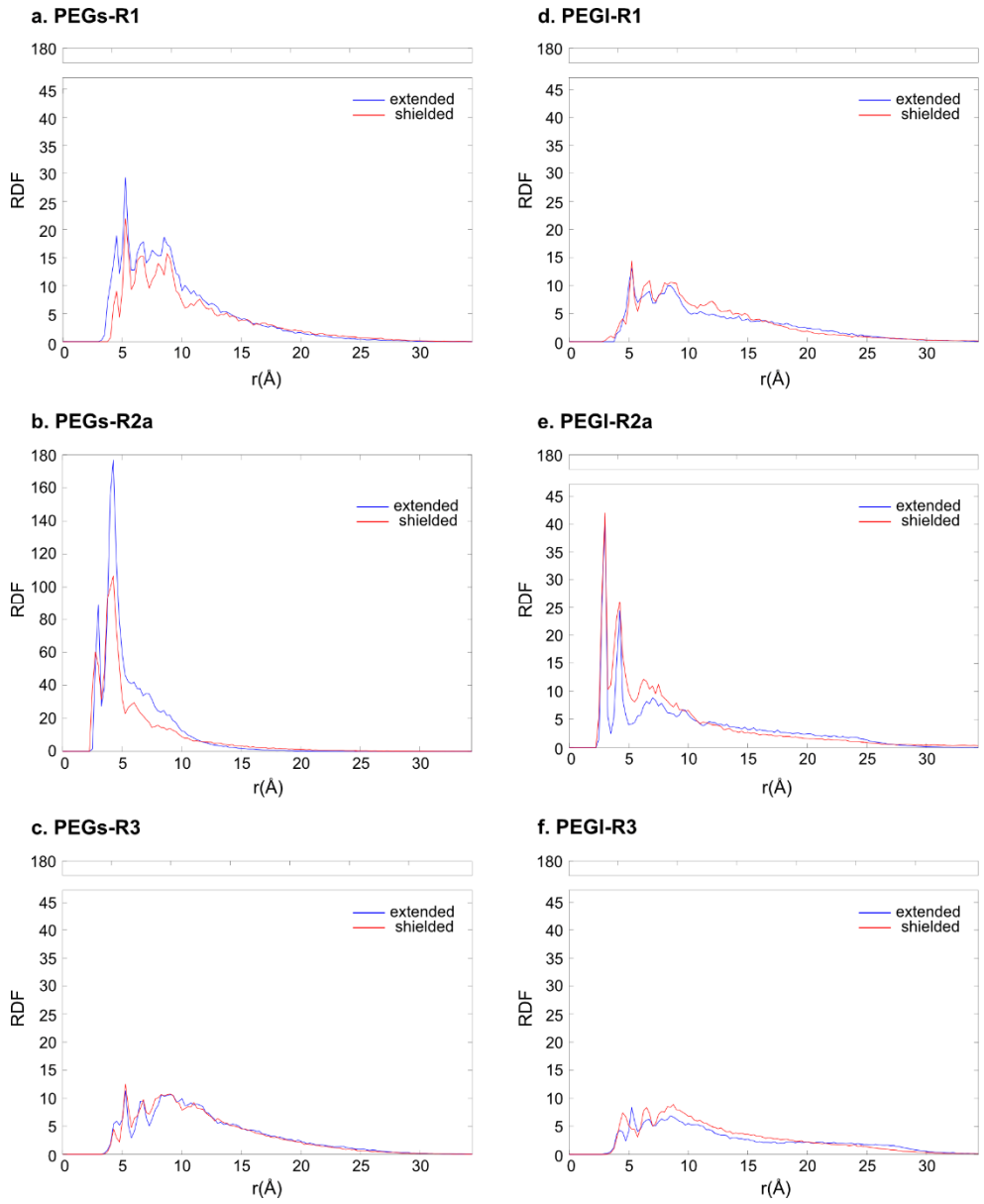

Figure 7. RDF of the PEG Os around polyamine Ns for the final 50 ns of the DNA binding simulations of **(a)** PEGs-R1, **(b)** PEGs-R2a, **(c)** PEGs-R3, **(d)** PEGl-R1, **(e)** PEGl-R2a, **(f)** PEGl-R3 polymers. The two curves in each plot represents the two initial polymer conformations, extended (blue) and shielded (red).

We further investigated how PEG chain participates in this self-associative behavior. In **Figure *8***, we plot the percentage of time during which the PEG Os are in close contact (within 4 Å) with polyamine Ns in the R2a systems. In all systems, the terminal O in the PEG chain, i.e., the

O atom closest to the polyamine group (O14 in short and O25 in long PEG chain, see the numbering in Figure 1a), is in close contact with at least one polyamine N at all times during the final 50 ns of the simulations. Previous analysis has shown that N1 of the R2a polyamine group is making a permanent contact with the PEG chain within the last 50 ns period (Figure 6b), indicating that the H-bond interaction of the N1–O14 or N1–O25 pair is mainly responsible for the intrachain associations in the R2a systems. The charged amine in the polyamine group immediately adjacent to the -OH group in the PEG-based chain creates a strong intramolecular, short-range "lock" between the polyamine and PEG groups, leading to a "collapsed" conformation which precludes effective interactions with DNA. Here, the polymer collapse is defined based on the decrease in the R_g of the polymers in the polymer–DNA simulations. The chain dimensions of the polymers comprising the R2a group have a higher tendency to be on the lower end of the sampled R_g range (5-22 Å); this effect is more prominent in the polymers with short PEG chains (Figure S9, Supporting Information). The length of the PEG chain determines the pattern of the intrachain associations: in polymers with the long PEG chain (Figure 8b), the strength of intrachain associations is progressively weakened farther away from the polyamine group; however, in the polymers comprising short PEG chain (Figure 8a), the middle region of the chain maintains a moderate amount of interactions with the polyamine group. This behavior is illustrated in Figure S10 (Supporting Information), where the proposed configurations of the PEG chain around the polyamine group R2a in explicit water are schematically illustrated. The weaker intrachain association observed in the polymers with long PEG chain further confirms the short-range nature of the H-bond between the polyamine N1 and adjacent PEG O14/O25. Due to this short-range attraction between the polyamine and PEG blocks, hydrophilic interactions between the long PEG

chain and water may dominate the intrachain associations within the polymers, thereby leading to larger polymer chain dimensions.

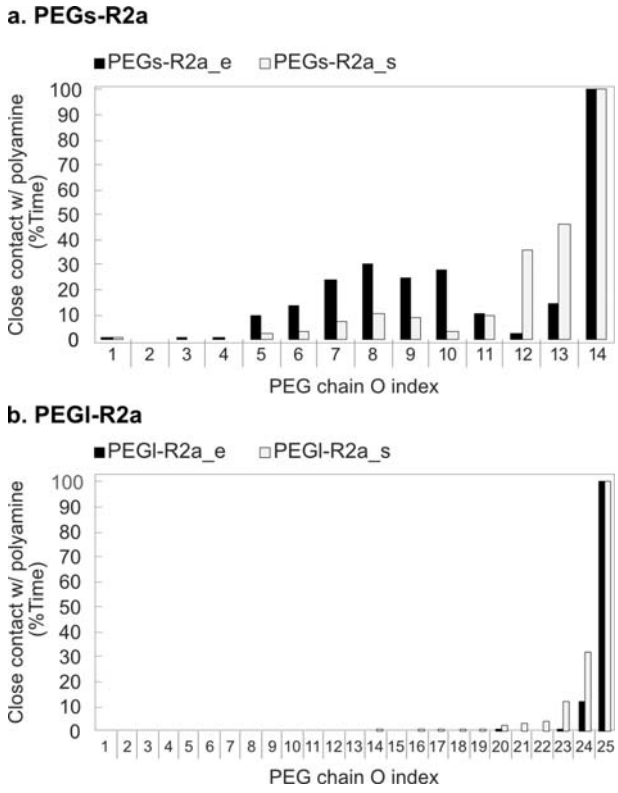

Figure 8. Percentage of time in which PEG chain Os are in close contact with polyamine Ns in the final 50 ns of the DNA binding simulations of **(a)** PEGs-R2a and **(b)** PEGl-R2a polymers. The numbering of the PEG Os is given in Figure 1a. O1 represents the oxygen farthest from the polyamine group, whereas O14/O25 is the closest.

3.2.2. The effect of unprotonated amine in the polyamine group

Taken together, the above findings suggest that the collapsed conformation of the polymers comprising R2a is the result of a strong H-bond interaction between the polyamine group N1 and the immediately adjacent PEG O14/O25. However, it is not clear if blocking this intrachain contact would restore polymer's DNA binding performance as R2a has another important architectural difference from R1 and R3: an unprotonated N between the cationic amine groups. As explained in Section 3.1, the unprotonated N has an impact on the DNA binding profile of the polyamine

group, however, the significance of this cannot be assessed in the presence of strong self-association within the polymer. To eliminate the structural bias towards intramolecular associations in the polymers comprising R2a, we designed a new polyamine group, R2b, by introducing a $–CH_2-CH_2–$ group to the left end of R2a (depicted in Figure 1b), as was done when designing R1 and R3.

We monitored the binding of R2b to DNA by varying the PEG chain length and polymer initial conformation (see Figure S11 in Supporting Information for the initial and final configurations of the R2b–DNA systems) and compared the DNA binding of R2b systems to those of R2a and R1 (Figure 9a). Our previous observations indicated a structural and conformational restraint on the R2a systems with regards to their DNA binding, i.e., R2a systems needed a short PEG chain and extended initial conformation to perform equivalently/slightly better than R1, and all other scenarios led to poor DNA binding. This pattern was also conserved in the R2b polymers, with only PEGs-R2b_e displaying better DNA binding than R1. This suggests that branching the architecture in small polyamine groups (R2a and R2b) without increasing the cationic charge is inferior over fully charged linear structure (R1). Comparing the DNA binding strength of R2a and R2b, it can be seen that, R2b binds DNA stronger than R2a.

The overall pattern of the interactions between the individual amines of the R2b group and DNA (Figure 9b) closely follows that of R2a: the unprotonated N, N0, forms the least amount of contacts, followed by N1; N2 and N3 are mostly responsible for binding to DNA. On average, the strength of interactions between individual polyamine Ns and DNA seem to be elevated in R2b when compared to R2a (Figure 5b), with the exception of N2 which maintains a similar level of interactions. Therefore, the addition of $–CH_2-CH_2–$ does not change the DNA binding profile of the polyamine group; however, it enhances the interactions of individual amines with DNA.

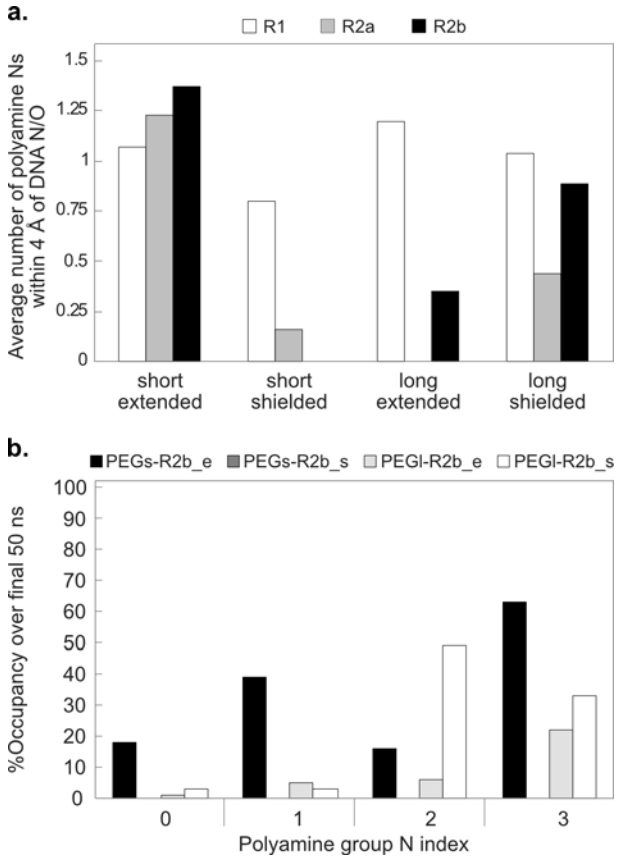

Figure 9. (a) Number of polyamine Ns within 4 Å of DNA N/O averaged over the final 50 ns of the simulations with R1, R2a, and R2b. **(b)** Percentage of time in which polyamine Ns are in close contact with DNA N/O in the final 50 ns of the simulations of the R2b systems. The numbering of the polyamine group Ns is given in Figure 1b.

We further assessed the self-associative behavior in the polymers comprising the R2b polyamine group. It can be seen that the added $–CH_2\text{-}CH_2–$ group significantly decreased the intrachain contacts made by N0 and N1, without affecting N2 and N3 (comparing Figure 10a to Figure 6b). This suggests that the self-association tendency of N2 and N3 is inherent to the architecture of the R2 polyamine group. Despite the significant reduction, the amount of intrachain association in R2b systems, particularly in the polymers with short PEG chain, is more than that in R1 (Figure 6a) and R3 (Figure 6c). The analysis of RDF of the PEG Os around polyamine Ns (Figure 10b) underpinned these observations. In comparison to R2a (Figure 7b, e), R2b systems displayed a substantially weaker first peak at 2.75 Å, indicative of the marked elimination of the

short range “lock”, followed by more prominent peaks at 4.25 Å and 5.25 Å. While the probability of finding a PEG O within the neighboring region of the polyamine Ns is much less in the R2b systems when compared to R2a, it is still higher than those in R1 and R3, particularly when the R2b group is attached to a short PEG chain (note the change in y-scale in PEGs-R2b shown in Figure 10b, left panel). In further support of this observation, the second half of the PEG chain (O7-O14) displayed low level (≤ 20%) of intrachain associations in the R2b systems with short PEG chain, whereas the systems with long PEG chain exhibited little to no intrachain contacts (Figure 10c).

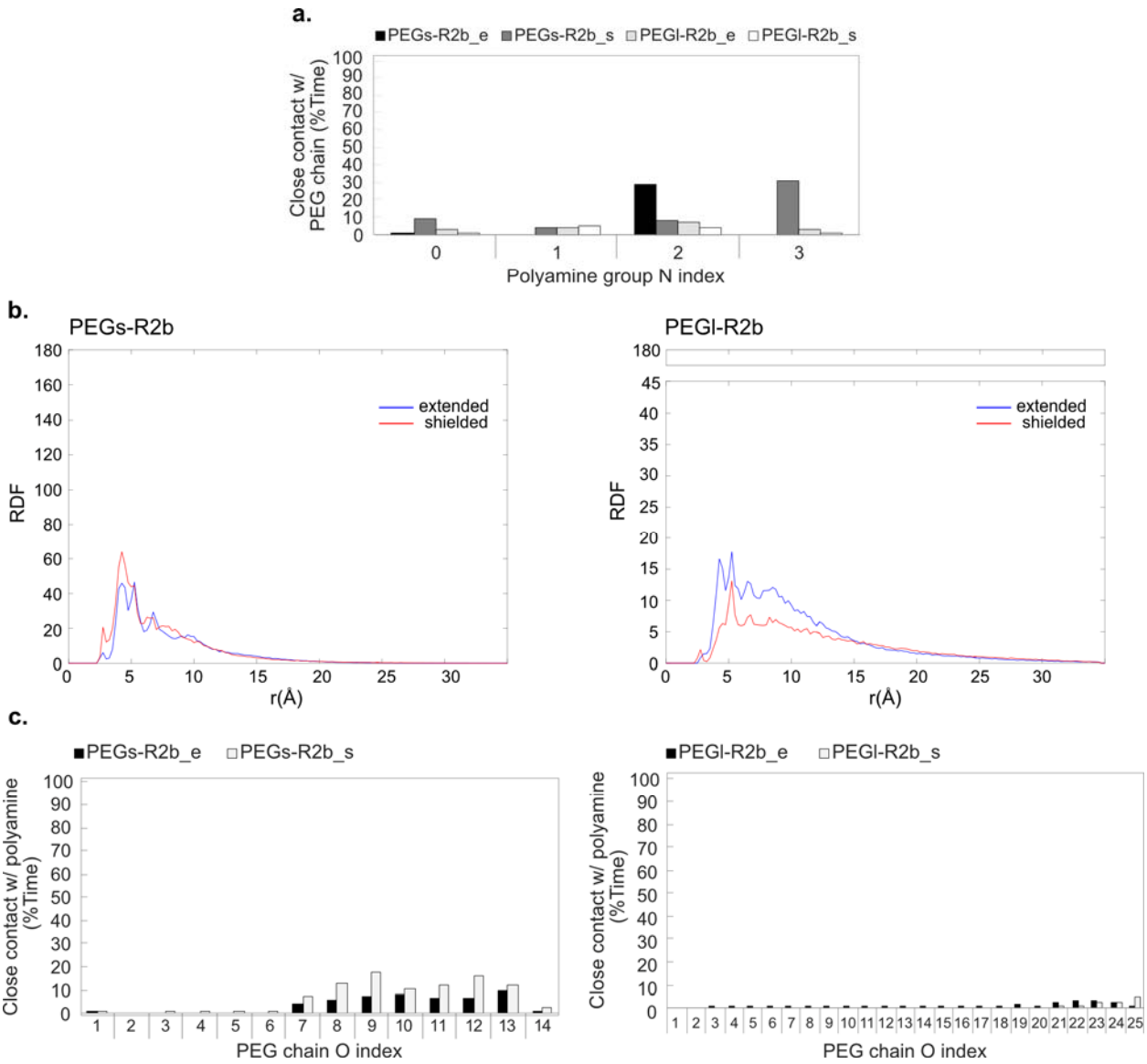

Figure 10. Polymer self-association in the R2b systems**. (a)** Percentage of time in which polyamine Ns are in close contact with PEG Os. **(b)** RDF of PEG Os around polyamine Ns. The two curves in each plot represents the two initial polymer conformations, extended (blue) and shielded (red). **(c)** Percentage of time in which PEG Os are in close contact with polyamine Ns. All the presented data are average values over the final 50 ns of the simulations.

Taken together, these considerations point to a structural basis for the separation of the PEG-R2a polymers from DNA in which the effects from (i) the absence of the –CH_2-CH_2– group before the polyamine block, and (ii) the presence of an unprotonated N in a semi-branched polyamine group architecture are coupled. The former creates a short-range lock via an internal O···H-N H-

bond between the O14/O25 of the PEG chain -OH and H-N1 of the polyamine group by placing these two groups at a close distance of 2.9–3.3 Å (Figure 11b). Although this distance falls within the broad range of bond length for normal/weak H-bonds, presence of cations in the H-bonds may increase their strength.[42] Due to the cationic charge of the tertiary amine, the -OH is proposed to act as the proton acceptor in this interaction, and H-N1 serves as the donor. It is known that -OH groups tend to act as H-bonding donors,[43] however it is possible for them to serve as proton acceptors when faced with proton donors.[44,45] This intramolecular H-bond interaction is absent in the polymers comprising R2b, as well as R1 and R3. The distance between the O14/O25 and N1 ranges from 5.1 to 5.3 Å in the R2b, and 4.9 to 5.7 Å in R1 and R3 systems (on average based on the final 50 ns, depicted in Figure 11), which is beyond the 3–4 Å cut-off for an H-bond. The –CH_2-CH_2– group preceding the first tertiary amine of R2b, R1, and R3 places N1 farther away from O14/O25, thus significantly eliminates the polyamine-PEG associations.

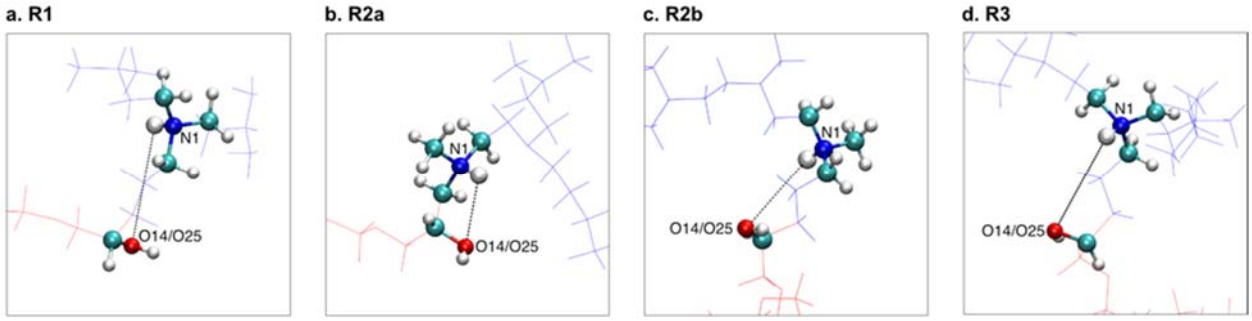

Figure 11. A schematic illustrating the distance between O14/O25 of the PEG chain and H-N1 of the polyamine group **(a)** R1, **(b)** R2a, **(c)** R2b, and **(d)** R3. The -OH group of the PEG chain and the tertiary amine of the polyamine group containing N1 are shown as spheres, while the remainder of the PEG chain and polyamine group are shown as red and blue lines, respectively. The color coding of the sphere representation of the atoms is as follows: cyan, C; red, O; blue, N; white, H.

The effects of the unprotonated N are manifested in two ways. Firstly, the presence of the unprotonated N in a semi-branched polyamine group allows only 2 out of 3 protonated amines (N2 and N3) to interact with DNA at a time, as the binding of all the charged amines to DNA is at the

expense of distorting the bonds between the amine groups. This poor electrostatic attraction between the polymer and DNA causes weaker binding and separation of the two. Secondly, N2 and N3 only weakly interact with DNA due to structural restraints, and this causes these two N atoms to be drawn towards the polymer PEG chain at times, particularly when the PEG chain is short, which leads to weak intrachain associations.

4. IMPLICATIONS

The inherent assumption in polymeric structures designed to arrest thrombosis is that polymers with strong nucleic acid binding capability stabilize the nucleic acid–polymer complex and minimize the blood clotting events, whilst this binding itself might not be the sole reason for the antithrombotic response *in vivo*.[22] The R2a polyamine group simulated in this work is identical to the trivalent polyP-binding polyamine group (R group) explored in the *in vitro* and *in vivo* experiments by Travers *et al.*[22], where a number of identical R groups are grafted to a dendritic polymer core. In a high-throughput screen of the potential polyP inhibitors, Travers and coworkers identified most potent polyP inhibitors with at least 5 or more R groups. Moreover, they observed inhibitors possessing lower cationic charge (7 R groups) being less effective than their higher charge counterparts (11 R groups) in terms of their *in vivo* antithrombotic activity, indicating that cationic charge of polymers is associated with polymer antithrombotic activity to some extent. Our simulations revealed that polymers interact with DNA mainly through their charged groups, and increasing the number of protonated tertiary amines in the polyamine group strengthens polymer-DNA binding. These observations correlate well with the reported experimental outcomes, and suggest that stronger electrostatic attraction between polymer and DNA may account for enhanced antithrombotic activity of the polymer.

What remains to be explored from MD simulation perspective is the behavior of the R2a polyamine group when grafted to a dendritic polymer core shielded with PEG chains, as in the UHRA compounds. The binding of cfNAs to R2a-containing polymers is expected to differ when R2a is connected to a single PEG chain vs. a more rigid and bulky dendritic structure. From isothermal titration calorimetry experiments, Shenoi *et al.* reported that dendritic UHRAs exhibit a few orders of magnitude higher binding affinity to unfractionated heparin than that of the methoxy PEG-R chain.[24] When R2a is attached to a dendritic core, the "locking" of the polyamine group via intrachain associations could still take place if the short distance between PEG O and protonated tertiary amine of the polyamine group is preserved. However, this interaction may not dominate the attractive forces to cfNA anymore as UHRA structures comprise multiple R groups,[22,24] which might be sufficient to drive polymer-DNA binding, as opposed to only one R in the polymers simulated in this work. Improving the structure of the R group to obtain stronger DNA binding is essential to decreasing the number of R groups per polymer required to generate an effective antithrombotic. Having less but more effective R groups is a key to enhancing the biocompatibility of the polymeric inhibitors.[25] *In vitro* and *in vivo* testing of the designed R groups will help understand the antithrombotic activity under physiological conditions.

5. CONCLUSIONS

We investigated DNA duplex binding of the polymers designed to have four different cationic polyamine groups, two different PEG-chain lengths, and two distinct initial conformations by carrying out systematic all-atom MD simulations, accumulating a total simulation time of 4 μs. Our results indicated that polyamine-PEG diblock polymers bind DNA mainly through the interactions of the cationic polyamine group with DNA backbone phosphate Os. While PEG-based chain did not take part in DNA binding, it was found to modulate the DNA binding profile of the

polyamine group. Increasing the number of protonated tertiary amines in the polyamine group enhanced the interactions with DNA. When the number of tertiary amine groups was increased while keeping the same cationic charge (partially protonated system) in a semi-branched polyamine group architecture, polymer–DNA binding was decreased disproportionately. Further analysis has shown that when significantly higher levels of polymer intrachain associations exist, polymer binding to DNA is adversely affected, and polymers separate from DNA. What gives rise to strong intrachain associations is the absence of a spacer (–CH_2-CH_2–) group in one of the partially protonated semi-branched polyamine group structure, causing a local conformational constraint that positions the PEG chain in the proximity of the polyamine group. Inserting the spacer –CH_2-CH_2– group improved polymer's DNA binding performance slightly; however, the polymer still performed poorly in comparison to the fully protonated systems. This was attributed to the presence of the unprotonated N amongst the charged amines, which limits the number of protonated Ns interacting with DNA since binding of all the protonated Ns to DNA would have caused major distortions in the bonds between the amine groups. Such a conformational restraint not only causes poor electrostatic attraction to DNA, but also leads to some degree of polymer intrachain associations, both undesired for polymer–DNA binding. The present study provides much-needed understanding into the design principles of diblock polymers toward superior DNA binding. The knowledge gained in this study will help advance the design of biocompatible and safe antithrombotic polymers to arrest DNA-induced thrombosis.

ACKNOWLEDGEMENTS

Compute Canada and Westgrid are gratefully acknowledged for providing the computing resources and technical support. This work is funded by Natural Sciences and Engineering Research Council of Canada (JNK, TT (RGPIN 341907), HU), NSERC Collaborative Research and Training Experience Program for Regenerative Medicine (JNK, HU), Canadian Institutes of Health Research (HU, JNK). JNK is a recipient of a Michael Smith Foundation for Health Research (MSFHR) Scholar Award.

Supporting Information

Parameterization of the polymers, equilibration of the polymers, initial configuration of the polymer–DNA simulation systems, time evolution of the polymer polyamine group and PEG chain binding to DNA, details of the intermolecular contacts between the polymer polyamine group and DNA, time series of the intramolecular contacts within the polymers in their DNA binding simulations, histograms of the radius of gyration of the polymers obtained from their DNA binding simulations, proposed conformations of the PEG chain around R2a polyamine group, and initial configurations of the R2b–DNA simulations.

REFERENCES

(1) Rickles, F. R.; Edwards, R. L. Activation of Blood Coagulation in Cancer: Trousseau's Syndrome Revisited. *Blood* **1983**, *62* (1), 14–31.

(2) Francis, J. L.; Biggerstaff, J.; Amirkhosravi, A. Hemostasis and Malignancy. *Semin Thromb Hemost* **1998**, *24*, 93–109.

(3) Prandoni, P.; Lensing, A. W. A.; Piccioli, A.; Bernardi, E.; Simioni, P.; Girolami, B.; Marchiori, A.; Sabbion, P.; Prins, M. H.; Noventa, F.; Girolami, A. Recurrent Venous Thromboembolism and Bleeding Complications During Anticoagulant Treatment in Patients with Cancer and Venous Thrombosis. *Blood* **2002**, *100* (10), 3484–3488.

(4) Hisada, Y.; Geddings, J. E.; Ay, C.; Mackman, N. Venous Thrombosis and Cancer: From Mouse Models to Clinical Trials. *Journal of Thrombosis and Haemostasis* **2015**, *13* (8), 1372–1382.

(5) Geddings, J.; Mackman, N. New Players in Haemostasis and Thrombosis. *Thromb Haemost* **2014**, *111*, 570–574.

(6) Renné, T.; Schmaier, A. H.; Nickel, K. F.; Blomback, M.; Maas, C. In Vivo Roles of Factor XII. *Blood* **2012**, *120* (22), 4296–4303.

(7) Kannemeier, C.; Shibamiya, A.; Nakazawa, F.; Trusheim, H.; Ruppert, C.; Markart, P.; Song, Y.; Tzima, E.; Kennerknecht, E.; Niepmann, M.; Bruehl, von, M.-L.; Sedding, D.; Massberg, S.; Gunther, A.; Engelmann, B.; Preissner, K. T. Extracellular RNA Constitutes a Natural Procoagulant Cofactor in Blood Coagulation. *PNAS* **2007**, *104* (15), 6388–6393.

(8) Leon, S. A.; Shapiro, B.; Sklaroff, D. M.; Yaros, M. J. Free DNA in the Serum of Cancer Patients and the Effect of Therapy. *Cancer Res.* **1977**, *37*, 646–650.

(9) Kopreski, M. S.; Benko, F. A.; Kwak, L. W.; Gocke, C. D. Detection of Tumor Messenger RNA in the Serum of Patients with Malignant Melanoma. *Clin. Cancer Res.* **1999**, *5*, 1961–1965.

(10) Ng, E. K. O.; Tsui, N. B. Y.; Lam, N. Y. L.; Chiu, R. W. K.; Yu, S. C. H.; Wong, S. C. C.; Lo, E. S. F.; Rainer, T. H.; Johnson, P. J.; Lo, Y. M. D. Presence of Filterable and Nonfilterable mRNA in the Plasma of Cancer Patients and Healthy Individuals. *Clin. Chem.* **2002**, *48* (8), 1212–1217.

(11) Shapiro, B.; Chakrabarty, M.; Cohn, E. M.; Leon, S. A. Determination of Circulating DNA Levels in Patients with Benign or Malignant Gastrointestinal Diseases. *Cancer* **1983**, *51*, 2116–2120.

(12) Lee, A. Y. Y.; Peterson, E. A. Treatment of Cancer-Associated Thrombosis. *Blood* **2013**, *122* (14), 2310–2317.

(13) Jain, S.; Pitoc, G. A.; Holl, E. K.; Zhang, Y.; Borst, L.; Leong, K. W.; Lee, J.; Sullenger, B. A. Nucleic Acid Scavengers Inhibit Thrombosis Without Increasing Bleeding. *PNAS* **2012**, *109* (32), 12938–12943.

(14) Smith, S. A.; Mutch, N. J.; Baskar, D.; Rohloff, P.; Docampo, R.; Morrissey, J. H. Polyphosphate Modulates Blood Coagulation and Fibrinolysis. *PNAS* **2006**, *103* (4), 903–908.

(15) Müller, F.; Mutch, N. J.; Schenk, W. A.; Smith, S. A.; Esterl, L.; Spronk, H. M.; Schmidbauer, S.; Gahl, W. A.; Morrissey, J. H.; Renné, T. Platelet Polyphosphates Are Proinflammatory and Procoagulant Mediators in Vivo. *Cell* **2009**, *139* (6), 1143–1156.

(16) Smith, S. A.; Choi, S. H.; Collins, J. N. R.; Travers, R. J.; Cooley, B. C.; Morrissey, J.

H. Inhibition of Polyphosphate as a Novel Strategy for Preventing Thrombosis and Inflammation. *Blood* **2012**, *120* (26), 5103–5110.
(17) Nickel, K. F.; Ronquist, G.; Langer, F.; Labberton, L.; Fuchs, T. A.; Bokemeyer, C.; Sauter, G.; Graefen, M.; Mackman, N.; Stavrou, E. X.; Ronquist, G.; Renné, T. The Polyphosphate-Factor XII Pathway Drives Coagulation in Prostate Cancer-Associated Thrombosis. *Blood* **2015**, *126* (11), 1379–1389.
(18) Jones, C. F.; Campbell, R. A.; Brooks, A. E.; Assemi, S.; Tadjiki, S.; Thiagarajan, G.; Mulcock, C.; Weyrich, A. S.; Brooks, B. D.; Ghandehari, H.; Grainger, D. W. Cationic PAMAM Dendrimers Aggressively Initiate Blood Clot Formation. *ACS Nano* **2012**, *6* (11), 9900–9910.
(19) Fischer, D.; Li, Y.; Ahlemeyer, B.; Krieglstein, J.; Kissel, T. In Vitro Cytotoxicity Testing of Polycations: Influence of Polymer Structure on Cell Viability and Hemolysis. *Biomaterials* **2003**, *24*, 1121–1131.
(20) Dobrovolskaia, M. A.; Patri, A. K.; Simak, J.; Hall, J. B.; Semberova, J.; De Paoli Lacerda, S. H.; McNeil, S. E. Nanoparticle Size and Surface Charge Determine Effects of PAMAM Dendrimers on Human Platelets in Vitro. *Mol. Pharmaceutics* **2012**, *9* (3), 382–393.
(21) Jones, C. F.; Campbell, R. A.; Franks, Z.; Gibson, C. C.; Thiagarajan, G.; Vieira-de-Abreu, A.; Sukavaneshvar, S.; Mohammad, S. F.; Li, D. Y.; Ghandehari, H.; Weyrich, A. S.; Brooks, B. D.; Grainger, D. W. Cationic PAMAM Dendrimers Disrupt Key Platelet Functions. *Mol. Pharmaceutics* **2012**, *9* (6), 1599–1611.
(22) Travers, R. J.; Shenoi, R. A.; Kalathottukaren, M. T.; Kizhakkedathu, J. N.; Morrissey, J. H. Nontoxic Polyphosphate Inhibitors Reduce Thrombosis While Sparing Hemostasis. *Blood* **2014**, *124* (22), 3183–3190.
(23) Kalathottukaren, M. T.; Abraham, L.; Kapopara, P. R.; Lai, B. F. L.; Shenoi, R. A.; Rosell, F. I.; Conway, E. M.; Pryzdial, E. L. G.; Morrissey, J. H.; Haynes, C. A.; Kizhakkedathu, J. N. Alteration of Blood Clotting and Lung Damage by Protamine Are Avoided Using the Heparin and Polyphosphate Inhibitor UHRA. *Blood* **2017**, *129* (10), 1368–1379.
(24) Shenoi, R. A.; Kalathottukaren, M. T.; Travers, R. J.; Lai, B. F. L.; Creagh, A. L.; Lange, D.; Yu, K.; Weinhart, M.; Chew, B. H.; Du, C.; Brooks, D. E.; Carter, C. J.; Morrissey, J. H.; Haynes, C. A.; Kizhakkedathu, J. N. Affinity-Based Design of a Synthetic Universal Reversal Agent for Heparin Anticoagulants. *Sci. Transl. Med.* **2014**, *6* (260), 260ra150.
(25) Kalathottukaren, M. T.; Abbina, S.; Yu, K.; Shenoi, R. A.; Creagh, A. L.; Haynes, C.; Kizhakkedathu, J. N. A Polymer Therapeutic Having Universal Heparin Reversal Activity: Molecular Design and Functional Mechanism. *Biomacromolecules* **2017**, *18*, 3343–3358.
(26) Sun, C.; Tang, T.; Uludağ, H.; Cuervo, J. E. Molecular Dynamics Simulations of DNA/PEI Complexes: Effect of PEI Branching and Protonation State. *Biophys. J.* **2011**, *100* (11), 2754–2763.
(27) Hart, K.; Foloppe, N.; Baker, C. M.; Denning, E. J.; Nilsson, L.; MacKerell, A. D., Jr. Optimization of the CHARMM Additive Force Field for DNA: Improved Treatment of the BI/BII Conformational Equilibrium. *J. Chem. Theory Comput.* **2012**, *8*, 348–362.
(28) Vanommeslaeghe, K.; Hatcher, E.; Acharya, C.; Kundu, S.; Zhong, S.; Shim, J.; Darian, E.; Guvench, O.; Lopes, P.; Vorobyov, I.; MacKerell, A. D., Jr. CHARMM General

Force Field: a Force Field for Drug-Like Molecules Compatible with the CHARMM All-Atom Additive Biological Force Fields. *J. Comput. Chem.* **2010**, *31* (4), 671–690.
(29) MacKerell, A. D., Jr.; Bashford, D.; Bellott, M.; Dunbrack, R. L., Jr.; Evanseck, J. D.; Field, M. J.; Fischer, S.; Gao, J.; Guo, H.; Ha, S.; Joseph-McCarthy, D.; Kuchnir, L.; Kuczera, K.; Lau, F. T. K.; Mattos, C.; Michnick, S.; Ngo, T.; Nguyen, D. T.; Prodhom, B.; Reiher, W. E.; Roux, B.; Schlenkrich, M.; Smith, J. C.; Stote, R.; Straub, J.; Watanabe, M.; Wiórkiewicz-Kuczera, J.; Yin, D.; Karplus, M. All-Atom Empirical Potential for Molecular Modeling and Dynamics Studies of Proteins. *J. Phys. Chem. B* **1998**, *102* (18), 3586–3616.
(30) Phillips, J. C.; Braun, R.; Wang, W.; Gumbart, J.; Tajkhorshid, E.; Villa, E.; Chipot, C.; Skeel, R. D.; Kalé, L.; Schulten, K. Scalable Molecular Dynamics with NAMD. *J. Comput. Chem.* **2005**, *26* (16), 1781–1802.
(31) Darden, T.; York, D.; Pedersen, L. Particle Mesh Ewald: an N · Log(N) Method for Ewald Sums in Large Systems. *J. Chem. Phys.* **1993**, *98* (12), 10089–10092.
(32) Ryckaert, J.-P.; Ciccotti, G.; Berendsen, H. J. C. Numerical Integration of the Cartesian Equations of Motion of a System with Constraints: Molecular Dynamics of *N*-Alkanes. *J. Comput. Phys.* **1977**, *23*, 327–341.
(33) Humphrey, W.; Dalke, A.; Schulten, K. VMD: Visual Molecular Dynamics. *J Mol Graph* **1996**, *14*, 33–38.
(34) Mafi, A.; Abbina, S.; Kalathottukaren, M. T.; Morrissey, J. H.; Haynes, C.; Kizhakkedathu, J. N.; Pfaendtner, J.; Chou, K. C. Design of Polyphosphate Inhibitors: a Molecular Dynamics Investigation on Polyethylene Glycol-Linked Cationic Binding Groups. *Biomacromolecules* **2018**, *19*, 1358–1367.
(35) Korolev, N.; Lyubartsev, A. P.; Nordenskiöld, L.; Laaksonen, A. Spermine: an "Invisible" Component in the Crystals of B-DNA. a Grand Canonical Monte Carlo and Molecular Dynamics Simulation Study. *J. Mol. Biol.* **2001**, *308*, 907–917.
(36) Korolev, N.; Lyubartsev, A. P.; Laaksonen, A.; Nordenskiöld, L. On the Competition Between Water, Sodium Ions, and Spermine in Binding to DNA: a Molecular Dynamics Computer Simulation Study. *Biophys. J.* **2002**, *82* (6), 2860–2875.
(37) Korolev, N. A Molecular Dynamics Simulation Study of Oriented DNA with Polyamine and Sodium Counterions: Diffusion and Averaged Binding of Water and Cations. *Nucleic Acids Res.* **2003**, *31* (20), 5971–5981.
(38) Korolev, N.; Lyubartsev, A. P.; Laaksonen, A.; Nordenskiöld, L. A Molecular Dynamics Simulation Study of Polyamine- and Sodium-DNA. Interplay Between Polyamine Binding and DNA Structure. *Eur Biophys J* **2004**, *33*, 671–682.
(39) Korolev, N.; Lyubartsev, A. P.; Laaksonen, A.; Nordenskiöld, L. Molecular Dynamics Simulation Study of Oriented Polyamine- and Na-DNA: Sequence Specific Interactions and Effects on DNA Structure. *Biopolymers* **2004**, *73*, 542–555.
(40) Sun, C.; Tang, T.; Uludağ, H. Molecular Dynamics Simulations for Complexation of DNA with 2 kDa PEI Reveal Profound Effect of PEI Architecture on Complexation. *J. Phys. Chem. B* **2012**, *116*, 2405–2413.
(41) Ziebarth, J.; Wang, Y. Molecular Dynamics Simulations of DNA-Polycation Complex Formation. *Biophys. J.* **2009**, *97* (7), 1971–1983.
(42) Jeffrey, G. A.; Saenger, W. *Hydrogen Bonding in Biological Structures*; Springer-Verlag: Berlin Heidelberg, 1994.
(43) Baker, E. N.; Hubbard, R. E. Hydrogen Bonding in Globular Proteins. *Prog. Biophys.*

Mol. Biol. **1984**, *44*, 97–179.
(44) Takeuchi, H.; Watanabe, N.; Satoh, Y.; Harada, I. Effects of Hydrogen Bonding on the Tyrosine Raman Bands in the 1300-1150 Cm^{-1} Region. *J. Raman Spectrosc.* **1989**, *20*, 233–237.
(45) Bohm, H.-J. LUDI: Rule-Based Automatic Design of New Substituents for Enzyme Inhibitor Leads. *J Comput Aided Mol Des* **1992**, *6*, 593–606.

Table of Contents (TOC)/Abstract Graphic